Biophysical Journal
Article

Biophysical Society

Monitoring Quantitative Ultrasound Parameter Changes in a Cell Pellet Model of Cell Starvation

Lauren A. Wirtzfeld,[1] Elizabeth S. L. Berndl,[1] Gregory J. Czarnota,[2] and Michael C. Kolios[1,*]
[1]Department of Physics, Ryerson University, Toronto, Ontario, Canada and [2]Departments of Radiation Oncology and Imaging Research, Sunnybrook Health Sciences Centre, and the Departments of Radiation Oncology and Medical Biophysics, University of Toronto, Toronto, Ontario, Canada

ABSTRACT Although it has previously been shown that the spectral analysis of ultrasound backscatter data is sensitive to the cellular changes caused by apoptosis, the sensitivity of spectral analysis to oncosis or ischemic cell death had not previously been studied. Whereas many anticancer treatments induce apoptosis, others induce cell starvation, or oncosis. HT-29 colon adenocarcinoma cells were formed into pellets and covered in phosphate-buffered saline at room temperature for 56 h. The pellets were imaged every 8 h with high-frequency (55 MHz) ultrasound and the raw radio-frequency data processed. The lack of nutrients available to the cells induced cell death due to oncosis. The attenuation slope, speed of sound, spectral slope, and midband fit were estimated at each of the eight time points to identify changes as the cells died due to starvation. The spectral slope decreased monotonically over the 56 h, whereas the attenuation slope showed an increase between 1 and 48 h, followed by a slight decrease between 48 and 56 h. The midband fit did not vary over time. The speed of sound increased from 1514 to 1532 m/s over the first 24 h, after which time it plateaued. These in vitro results indicate different trends in ultrasound parameter changes from those of in vitro apoptotic cells, suggesting that these different methods of cell death can be identified not only by morphological markers, but also by specific ultrasound signatures.

INTRODUCTION

The noninvasive monitoring and detection of changes in tissue microstructure would have significant impact on the assessment of clinical procedures and treatments, particularly in the field of oncology. Conventional B-mode ultrasound imaging uses the log-compressed envelope of the receive radio-frequency (RF) signal to create an image for viewing. This approach results in the loss of the frequency-dependent spectral information that contains information on the subwavelength microstructure of the scattering media (1). Quantitative ultrasound techniques, in particular attenuation- and power-spectra-based parameters, are believed to change based on the cellular size, shape, and morphology (2–5). As all of these aspects change based on cellular states, it is theorized that quantitative ultrasound can be used to identify and differentiate cellular growth, stasis, apoptosis, and oncosis. Both apoptosis and oncosis lead to necrosis, which is the degradation of cells after cell death (2,3). This distinction between the method of cell death and the final state of necrosis is sometimes overlooked in the literature observing cell death (5).

Apoptosis, or programmed cell death, has been well characterized histologically, metabolically, and by using quantitative ultrasound as a result of its role in cell death after chemotherapeutics and radiation treatment on cancer cells. The stages of apoptotic cell death include nuclear condensation, and cell shrinkage due to blebbing (3–5).

Oncotic cell death is less well understood, and occurs primarily when cells are unable to maintain cell integrity due to lack of energy, for example, in situations such as ischemia or nutrient starvation. Although a basic understanding of the structural changes is available, the details of the molecular and metabolic changes have not been fully probed, nor have changes in quantitative ultrasound parameters. As described by Weerasinghe and Buja (2), the membranes of cells undergoing oncosis go through three stages: partial membrane permeability, irreversible membrane permeability, and membrane destruction.

During the oncotic stage of partial membrane permeability, cells have limited access to a resource (nutrients or oxygen), leading to partial permeability to ions and water due to the failure of the ATP-dependent Na^+-K^+ pumps. Cells start to swell in suspension and dissociate from flasks

Submitted October 11, 2016, and accepted for publication May 9, 2017.
*Correspondence: mkolios@ryerson.ca
Editor: Catherine Galbraith.
http://dx.doi.org/10.1016/j.bpj.2017.05.017

when grown in a monolayer, which is visible by microscopy as a more spherical, rounded cell structure (2,4). At this stage, which occurs as early as 1 h after nutrients are removed in vivo (3) or 5–10 h after nutrients are removed in vitro (4,5), adding more nutrients or oxygen will allow the cells to recover (4). Irreversible permeability of the cell membranes occurs after ~7 h in vivo (3), and 24 h in vitro (5). At this point the cells can no longer be rescued from the death pathway. The cells continue to swell and the cells lose their selective membrane permeability, allowing in much larger molecules such as trypan blue to traverse the cell membrane. Finally, a physical disruption of the cell membranes, occurring 48–72 h after nutrient removal, is the actual cause of death in oncosis (3–5). Oncosis also causes the endoplasmic reticulum, Golgi apparatus, and mitochondria to become enlarged and the nuclear chromatin to condense.

A direct comparison between oncotic and apoptotic cells was completed using acute myeloid lymphoma cells at room temperature. Changes in the cell structure observed by electron microscopy and in the ultrasound midband fit were reported due to cell swelling (6). The oncotic cells were not monitored beyond 5 h, giving an incomplete picture of the spectral changes due to oncosis. Over a longer period of time, optical coherence tomography, a complementary technique to ultrasound, was able to differentiate pellets undergoing different forms of cell death i.e., apoptosis, mitotic arrest, and mitotic catastrophe (7). This article is similarly interested in using high-frequency ultrasound to observe the stages of oncotic cell death.

Individual cells and cell pellets undergoing apoptosis due to chemotherapeutics have resulted in significant changes in ultrasound spectral parameters (8). Previous work has shown ultrasound contrast between viable and nutrient-depleted regions of spheroids (9,10) and tumors (11).

In this work, colon adenocarcinoma pellets were maintained for 56 h without nutrients. Ultrasound data were acquired every 8 h, with matched pellets used for histological analysis and viability assays. Cells underwent oncosis, and the changes in spectral ultrasound parameters (attenuation slope, speed of sound, spectral slope, and midband fit) were correlated with changes in membrane permeability, cell size, and nucleus size. Changes in ultrasound parameters due to oncosis are sufficiently different from those changes previously described for apoptosis and may be useful to determine the extent and type of cellular death in vivo.

MATERIALS AND METHODS

Pellet model

Colon adenocarcinoma cells (HT-29; ATCC, Manassas, VA) were grown in McCoy's 5A media (Gibco/Thermo Fisher Scientific, Waltham, MA; prepared at Princess Margaret Hospital, Toronto, Ontario, Canada), and supplemented with 10% fetal bovine serum (Gibco). Cells were maintained in the exponential growth phase, and passed twice a week until pellet preparation. Cells were grown at 37°C, 5% CO_2 in a humidified incubator.

For each pellet, HT-29 cells were dissociated with trypsin and 30,000,000 cells were placed in the well, and centrifuged for 10 min at 200 × g. Supernatant media was gently removed, and the pellets were covered with phosphate-buffered saline (PBS) (Gibco/Thermo Fisher Scientific; prepared at Princess Margaret Hospital) and placed at room temperature for the remainder of the experiment. A total of 22 cell pellets were prepared: 16 in individual 8-mm diameter flat-bottomed tubes for viability assays and histology (VH samples), and six in a custom stainless-steel holders with three wells of 3.02-mm depth and 7.8-mm diameter for ultrasound imaging. All six pellets in the stainless-steel holders had ultrasound data acquired 1, 8, 24, 32, 40, 48, and 56 h after the cells were dissociated from the flask. The remaining 16 VH samples were used, two at each time point, to provide time-matched data for live/dead cell counts and for histology.

Live/dead cell counts

At each time point, a VH sample was resuspended in PBS and trypan blue and cells were counted with a hemocytometer. In each of the eight assays, cells with impermeable membranes were considered alive, and those with permeable membranes, dead.

Histology and staining

At each time point, the PBS from a time-matched VH pellet was replaced with neutral buffered formalin to fix the pellet for 2–5 days. Each of the eight pellets were then put into paraffin blocks, and cut to 6-μm sections. For each time point, two sets of slides were prepared: Hoechst and Wheat Germ Agglutinin (WGA) AlexaFluor 594 (Invitrogen, Carlsbad, CA), and Hoechst and DeadEnd Fluorometric TUNEL (Promega, Madison, WI).

Hoechst and WGA staining. Slides stained with WGA were deparaffinized in xylene and a decreasing ethanol gradient, underwent antigen retrieval (10 mM sodium citrate), were blocked with 1% bovine serum albumin and 5% FBS in PBS, and then stained according to the protocol provided with the WGA kit, using PBS instead of Hanks balanced salt solution. After washing in PBS, cells were counterstained with Hoechst, sealed, and imaged with a model No. IX71 microscope (Olympus, Tokyo, Japan), using an X-cite 120 laser (Excelitas Technologies, Waltham, MA), and captured with an Evolution QEi monochromatic camera (Media Cybernetics, Silver Spring, MD) using Q Capture Pro 6.0 (QImaging, Surrey, British Columbia, Canada). WGA binds to sialic acid and N-acetylglucosaminyl residues, allowing for the identification of cell membranes, whereas Hoechst binds to DNA, allowing for identification of the nucleus.

Calculating cell-nucleus diameter ratios. Images from the WGA-stained slides were processed using the software ImageJ (12). Briefly, the Hoechst image for each slide was opened in gray-scale and a grid was applied. Any nucleus located at a grid intersection was selected for sizing. The nucleus was manually outlined, and the areas recorded. The matching gray-scale WGA image was then opened, and cells overlapping a measured nucleus were outlined, producing matched pairs of cell and nuclear areas, and estimated cell and nuclear diameters were calculated. For each cell, the ratio of cell diameter to nuclear diameter was calculated to determine a relative size of the cell. Between 20 and 45 cells and their nuclei were measured at each time point.

Hoechst and TUNEL staining. To determine the cause of cell death in the pellets, they were probed with TUNEL, which binds specifically to single-stranded breaks in DNA, characteristic of apoptotic cell death. Slides stained with TUNEL were deparaffinized, as above, and then processed according to the protocol provided with the DeadEnd Fluorometric TUNEL kit (Promega). Slides were counterstained with Hoechst. Positive controls were prepared using DNase I. Images were captured using the Olympus IX71 system described above.

Ultrasound data acquisition

Data were acquired with a Vevo 770 preclinical imaging system (VisualSonics, Toronto, Ontario, Canada) with a single-element mechanically scanning transducer with an f# 2.25, analyzed over a frequency range of 25–50 MHz with an approximate resolution of 60 × 92 μm resolution at the 4.5 mm focal depth. This system has a 420 MHz digitizer board digitizing samples at 12 bits per sample, which was used to collect raw RF data from the pellets. The pellets were imaged at each of the eight time points described above. At each time point, 12 planes of 100 scan-lines over a lateral width of 2 mm were acquired for each of the six pellets.

System-dependent effects were removed from the sample data using the established method of using a reference reflection to normalize spectral data (13). Reference data were acquired, with a 30-dB attenuator, from the stainless-steel bottom of the third well of the pellet holder (reflection coefficient of 0.94), which contained only PBS.

Ultrasound data processing

All ultrasound data were processed in MATLAB (The MathWorks, Natick, MA). Within reconstructed B-mode images of the pellet, the top and bottom were manually identified.

Attenuation. The attenuation through the pellet was estimated by first acquiring a reflection from the planar reflector at the bottom of the reference well and dividing its power spectrum by the power spectrum from the reflection of the planar reflector beneath the sample well for each scan line (14,15). The resulting ratio was divided by the pellet thickness at the same location. A linear fit over the transducer bandwidth (25–50 MHz) was performed, with the slope taken as the attenuation slope, which was averaged across scan lines to provide an estimate for each slice of data. The average attenuation slope estimate for each time point was used for attenuation compensation in the spectral analyses.

Speed of sound. The speed of sound (SOS) in the pellet was estimated using the time of flight to the bottom of the PBS-only reference well compared to the time of flight to the bottom of the sample well. The SOS in PBS was taken as a constant of 1500 m/s, and the SOS of the pellet was calculated as the following:

$$c_{\text{pellet}} = 2 * d/\Delta t, \quad (1)$$

where Δt is the difference in time between the echo from the top of the pellet (determined based on segmentation) and the planar reflector beneath the pellet (peak of the reflection) and d is the pellet thickness estimate calculated based on the top of the pellet and the known location of the depth of the well from the PBS-only reference well (6).

Power spectra. The RF data from the pellet was divided into regions of interest (ROIs) that were 10 pulse lengths by six beamwidths (20 scan lines) in size with 50% overlap both axially and laterally. Analyses were performed on a per-ROI basis allowing for attenuation compensation to the depth of the ROI and the local computation of parameters. First, the power spectrum received from the sample for each ROI was normalized by the average power spectrum from the received signal from the planar reflector by dividing the power spectra in linear units. To compensate for the signal loss due to attenuation through the cell pellets, the frequency-dependent attenuation based on the distance to the center of the ROI was estimated and added to the normalized power spectrum in dB.

Linear regression was performed on the attenuation-corrected and normalized power spectra to extract the spectral slope and midband fit parameters (13).

Statistical analysis

ANOVAs (Prism, GraphPad, CA) were performed for each of the quantitative parameters to determine if there were statistically significant differences observed as time progressed. A variable with a p value of <0.05 was considered significant and post hoc comparisons using Tukey's least significant differences identified 95% confidence intervals to determine pairs that were significantly different.

RESULTS

Live/dead cell counts

The number of living cells generally decreased over time, with the number of dead cells increasing. (Fig. 1 *A*) The total number of cells (living and dead), remained fairly constant, with $(21 \pm 2) \times 10^6$ cells counted at each time point. Cell mortality (Fig. 1 *B*) over time showed a stable fraction of living cells from 1 to 8 h, a plateau at 24–40 h, and a steep dropoff to 7% survival after 48 h.

Histology correlations

The cell/nucleus ratio, as determined by the ratio between the estimated diameter of cells and their nuclei, was generally constant, with the 24-h ratio statistically significantly larger than the measurements both before (1, 8, and 16 h) and after (40 h) this time point (Fig. 2).

None of the time points tested were positive for TUNEL (Fig. 3) staining, compared to the positive control, indicating the mode of cell death was not apoptosis.

B-mode ultrasound

Fig. 4 *A* presents representative reconstructed B-mode images of a pellet at 1-, 24-, and 56-h time points. Small

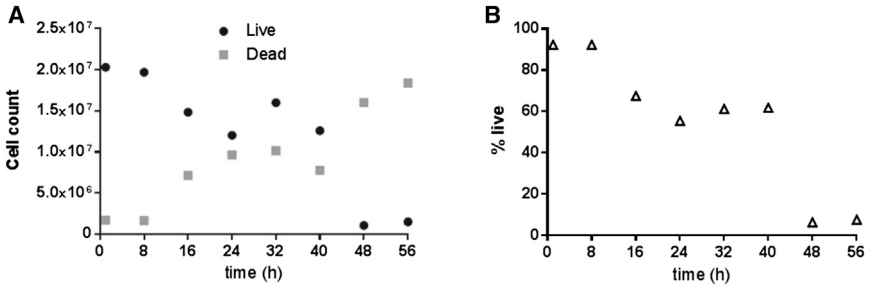

FIGURE 1 (*A*) Given here are total live and dead cell counts, as determined by trypan blue staining for each time point. (*B*) Given here is the percentage of cells alive in the cell pellet at each time point.

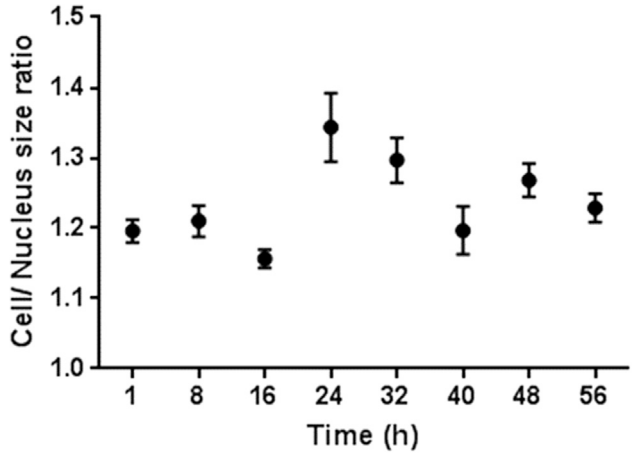

FIGURE 2 Shown here are the ratios between the estimated cell and nucleus diameters at each time point as mean ± SE. Larger values indicate a relative increase in cellular diameter.

differences are observable between the three B-mode images. The attenuation compensated and normalized power spectra from the pellets are plotted in Fig. 4 *B*, which demonstrate variations between the different time points not readily observable on the B-mode images.

Attenuation

Over time, the attenuation slope increased (Fig. 5, *left*) from 0.053 dB/mm MHz at 1 h to 0.073 dB/mm-MHz at 48 h. After the maximum at 48 h there was a slight decrease to 56 h. When comparing sequential time points, there are statistically significant differences in attenuation between 1 and 8 h, 8 and 16 h, and 32 and 40 h. All other neighboring time points do not have statistically significant differences from each other. The attenuation slope estimates demonstrate a gradual increase in value between 1 and 40 h, with the attenuation plateauing from 40 to 56 h.

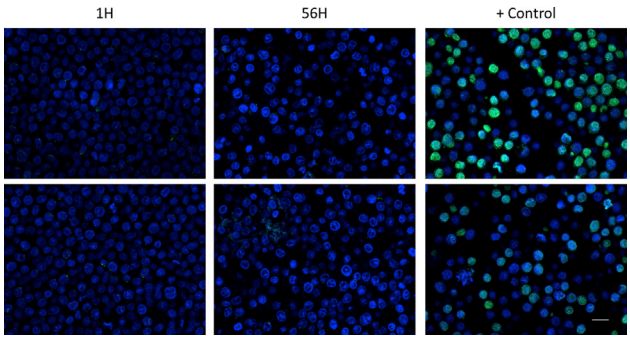

FIGURE 3 Given here are representative histological slides stained with DeadEnd Fluorometric TUNEL. Columns represent the 1-h time point, the final 56-h time point, and the positive control prepared with DNase I. No positive staining is seen at 1 or 56 h, indicating cell death is not via the apoptotic pathway. Scale bar is 20 μm for all images. To see this figure in color, go online.

Speed of sound

The SOS (Fig. 5, *right*) increased from 1514 m/s at 1 h to 1532 m/s at 24 h, after which the SOS plateaued. The 1-, 8-, and 16-h time points are statistically significant from each other, as well as from all points from 24 h onward. After the 24-h time point, there are no statistically significant differences between sequential speeds of sound.

Spectral slope

A monotonic decrease in the spectral slope was observed (Fig. 6, *left*), with a decrease from 0.73 dB/MHz at 1 h to 0.56 dB/MHz at 56 h. All time points were statistically significantly different from their neighbors, except between the 24- and 32-h and the 40- and 48-h time points.

Midband fit

The midband fit showed no statistically significant changes over time (Fig. 6, *right*) with values ranging from −31.88 to −32.32 dB. A slight increase in value is observed after 40 h, although still not being statistically significant.

DISCUSSION

Our study shows that cells dying due to oncosis can be identified using a set of quantitative ultrasound parameters. Because there was no evidence of TUNEL staining at 56 h, when 93% of the cells were dead, it is highly unlikely that the cells were dying through an apoptotic pathway. Similarly, the total number of cells remained consistent over the 56-h experiment, meaning that decay and cell disintegration due to necrosis had not yet occurred. We also observed swelling of cells at the 24-h time point, followed by the return to the initial size by 40 h after removal of nutrients. These physiological and morphological changes indicate that cell death occurred primarily using the oncotic pathway.

The cell mortality (Fig. 1 *B*) shows three distinct stages of cell death within this experiment, which appears to mimic the three stages of oncosis, as had been described in Weerasinghe and Buja (2). A previous in vitro study (4) showed that in nutrient-free conditions, fibroblasts growing in a monolayer had evidence of reversible membrane permeability after 10 h, irreversible permeability after 24 h, and that 50% of cells were positive for TUNEL staining after 48 h. This study shows similar time kinetics, with irreversible membrane permeability in the form of trypan-blue staining starting at 16 h after nutrient removal, and increasing to 97% permeable at 48 h. One major difference between the studies is that even after 56 h of starvation, cells remained TUNEL-negative in this study (Fig. 3).

Using the time stages observed in the cell mortality measurements, similar patterns can be found in both the

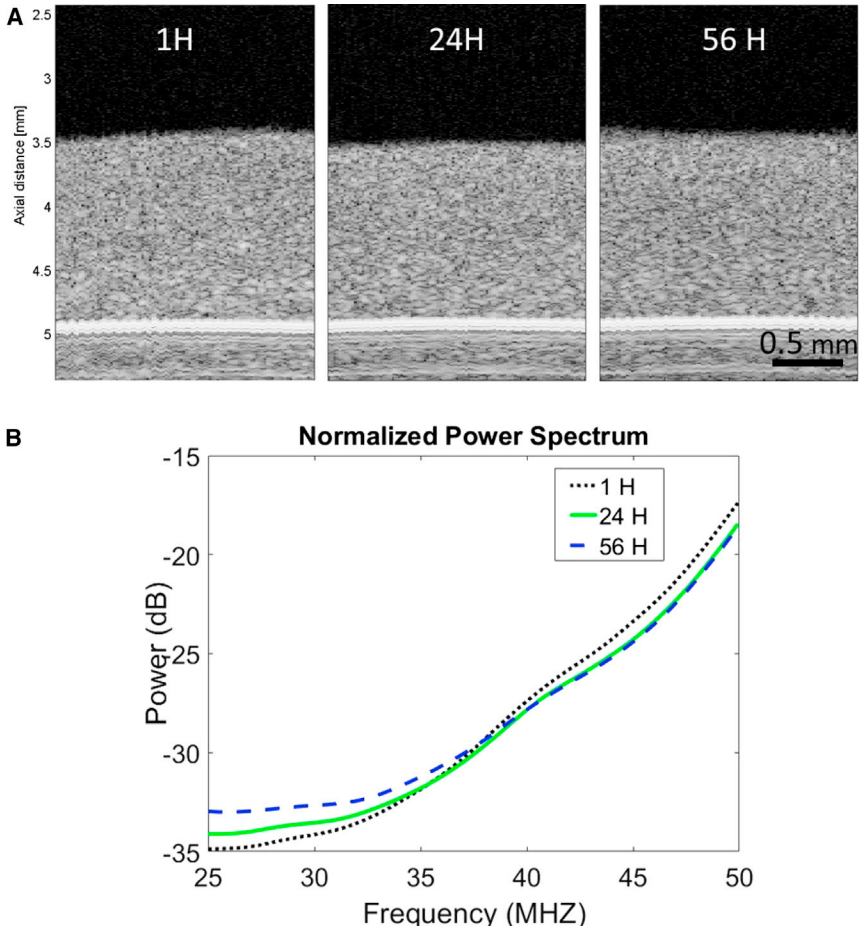

FIGURE 4 Shown here are B-mode images (*A*) and normalized power spectra (*B*) of pellets at 1-, 24-, and 56-h time points. To see this figure in color, go online.

attenuation and speed of sound. In attenuation, there was a rapid change during the first 16 h, followed by a more gradual increase to 40 h, after which there were no statistically significant changes. Speed of sound had a gradual increase to 24 h, and after which the speed of sound remained constant. The attenuation and speed of sound are generally measures of bulk properties of the medium and as such it is difficult to attribute such changes to particular morphological change in individual cells. The attenuation is a function of the medium's sound absorption and scattering, and the speed of sound is a function of the density and compressibility. Oncosis causes changes to the osmotic pressure of the cell, as well as the size and shape of the organelles. Each of these could have an effect on the bulk properties, absorption, and scattering of the cells. Variations between timing of stages between histology and ultrasound likely arise due to differences between the characteristics being observed. For example, the percentage of dead cells is determined by membrane permeability, and membrane permeability would not be directly detected with our ultrasound technique.

The data from the six imaged pellets were collected over two experiments performed at different times (two imaged

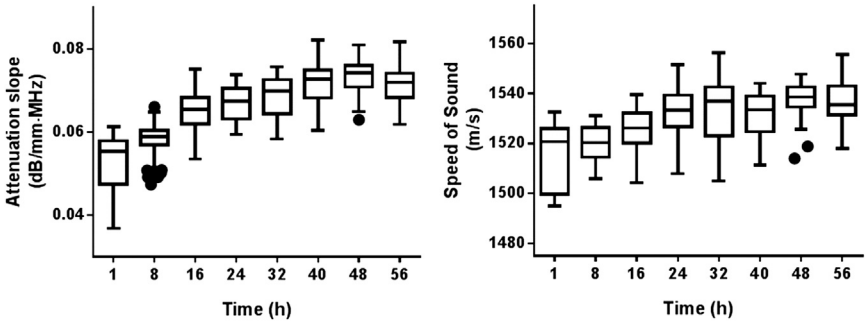

FIGURE 5 Given here are ultrasound estimates of the HT-29 cell pellet attenuation (*left*) and speed of sound (*right*) over time. Tukey box-and-whiskers graphs of all planes imaged from the imaging pellets are presented showing the median, 25th, and 75th percentile ranges with the boxes, and 1.5 times the interquartile range with the whiskers. Data points outside of the whiskers are shown as individual dots.

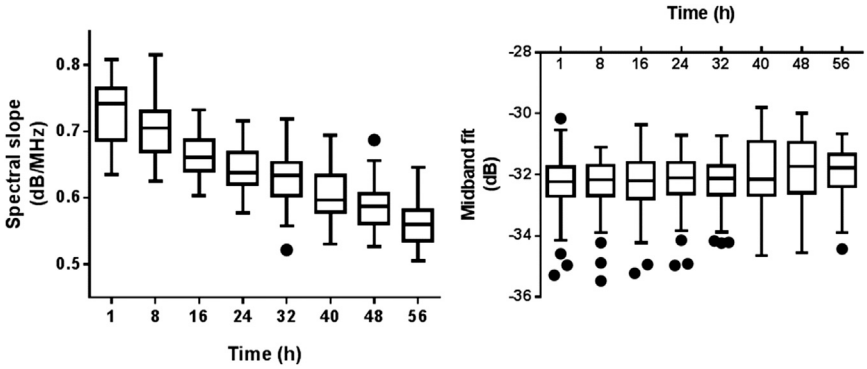

FIGURE 6 Given here are the spectral slope (*left*) and midband fit (*right*) estimates of HT-29 pellets over time. Tukey box-and-whiskers graphs of all planes imaged from the two imaging pellets are presented.

pellets in the first experiment and four imaged pellets in the second). As a result there is some natural variation that arises, when the cells are not all starting from the identical starting point. This may explain the overall larger variability in the initial time points.

At each time point, 54–64 planes of ultrasound data were acquired from the six pellets to provide enough data for analysis to ascertain the reproducibility of the ultrasound measurements for a given stage of oncosis. Timing and initial conditions of the samples are important, as minor variations in initial conditions can result in different oncosis kinetics.

We have shown a general trend of decreased spectral slope and uniform midband fit during oncosis. This differs from the trend of increased spectral slope and midband fit that has previously been shown in apoptosis (8). Further study directly comparing a variety of forms of cell death would be required to fully separate and identify them using noninvasive techniques.

Although we cannot unambiguously correlate ultrasound parameters to specific changes in the cellular architecture, there are a number of potential explanations for the observed changes. In general, a decrease in spectral slope would correlate to an increase in the effective scatterer size. The decrease measured in these experiments is consistent with observations that the cells swelled (increased in size) during the first 24 h of oncosis due to the loss of the selective membrane permeability. However, after the 24-h time point, the spectral slope continues to decrease, whereas the cells are observed to return to their initial size, perhaps indicating that the individual cell is not the dominant scattering source in the system, or that as the cells decreased in volume, they settled into a more organized pattern, which also can reduce the spectral slope (16,17). The lack of change in midband fit, unlike the results for apoptosis, may be due to the lack of significant changes in chromatin density for the majority of the process of oncosis, unlike what is observed for apoptosis.

In vivo, the changes in ultrasound characteristics would likely be similar for early time points, but would differ as oncosis progresses to necrosis due to immune cell involvement, a process not present in this in vitro experiment. The interest in different types of cell death arises from the heterogeneity of tumor response to treatment, both within a patient and between patients. Cells directly responding to chemotherapy and radiation treatment undergo apoptosis, but there can also be regions where the blood supply is disrupted and access to nutrients and oxygen limited, and when these cells die, they would undergo oncosis. Being able to identify the different types of cell death may provide information on what is happening at the cellular level within the tumor. Extended periods of nutrient deprivation, that do not result in cell death, are not desired due to cells adapting to hypoxic regions or becoming dormant and therefore resistant to conventional treatment.

CONCLUSIONS

Oncotic cell death caused unique changes in cellular microstructure, which resulted in consistent and distinct changes measured with high-frequency ultrasound, including attenuation slope, SOS, and spectral slope. These spectral parameters displayed gradual, monotonic changes during the first 40 h of the experiment, at which time the trends either continued, or plateaued. The ability to distinguish, using ultrasound, a variety of microstructural changes, including variations in the type of cell death, could provide additional clinical information on therapeutic responses in vivo.

AUTHOR CONTRIBUTIONS

L.A.W. contributed to the experimental design, data acquisition and data processing, and article writing. E.S.L.B. contributed to the experimental design, data acquisition and statistical analysis, and article writing. G.J.C. and M.C.K. contributed to the research design and article writing.

ACKNOWLEDGMENTS

This work is supported by the Terry Fox New Frontiers Program Project Grant in Ultrasound and MRI for Cancer Therapy (CIHR#TFF 105267). This research was undertaken, in part, thanks to funding from the Canada Research Chairs Program awarded to M.C.K. Funding to purchase the equipment was provided by the Canada Foundation for Innovation, the Ontario Ministry of Research and Innovation, and Ryerson University.

REFERENCES

1. Preface and state of the art methods for estimating backscatter coefficients. *In* Quantitative Ultrasound in Soft Tissues. J. Mamou and M. L. Oelze, editors. Springer, New York, pp. 3–19.
2. Weerasinghe, P., and L. M. Buja. 2012. Oncosis: an important non-apoptotic mode of cell death. *Exp. Mol. Pathol.* 93:302–308.
3. Majno, G., and I. Joris. 1995. Apoptosis, oncosis, and necrosis. An overview of cell death. *Am. J. Pathol.* 146:3–15.
4. Hasan, N. M., G. E. Adams, and M. C. Joiner. 1999. Effect of serum starvation on expression and phosphorylation of PKC-α and p53 in V79 cells: implications for cell death. *Int. J. Cancer.* 80:400–405.
5. van Cruchten, S., and W. van den Broeck. 2002. Morphological and biochemical aspects of apoptosis, oncosis and necrosis. *Anat. Histol. Embryol.* 31:214–223.
6. Kolios, M. C., L. Taggart, …, M. B. Sherar. 2003. An investigation of backscatter power spectra from cells, cell pellets and microspheres. 2003 IEEE Symposium on Ultrasonics, Honolulu, HI, October 5–8.
7. Farhat, G., V. X. D. Yang, …, M. C. Kolios. 2011. Detecting cell death with optical coherence tomography and envelope statistics. *J. Biomed. Opt.* 16:026017.
8. Kolios, M. C., G. J. Czarnota, …, M. D. Sherar. 2002. Ultrasonic spectral parameter characterization of apoptosis. *Ultrasound Med. Biol.* 28:589–597.
9. Sherar, M. D., M. B. Noss, and F. S. Foster. 1987. Ultrasound backscatter microscopy images the internal structure of living tumour spheroids. *Nature.* 330:493–495.
10. Wirtzfeld, L. A., E. S. L. Berndl, …, M. C. Kolios. 2014. Effective scatterer size estimates in HT-29 spheroids at 55 MHz and 80 MHz. 2014 IEEE International Ultrasonics Symposium, Chicago, IL, September 3–6.
11. Graham, K. C., L. A. Wirtzfeld, …, A. F. Chambers. 2005. Three-dimensional high-frequency ultrasound imaging for longitudinal evaluation of liver metastases in preclinical models. *Cancer Res.* 65:5231–5237.
12. Schneider, C. A., W. S. Rasband, and K. W. Eliceiri. 2012. NIH image to ImageJ: 25 years of image analysis. *Nat. Methods.* 9:671–675.
13. Lizzi, F. L., M. Greenebaum, …, D. J. Coleman. 1983. Theoretical framework for spectrum analysis in ultrasonic tissue characterization. *J. Acoust. Soc. Am.* 73:1366–1373.
14. Wear, K. A., T. A. Stiles, …, J. R. Yuan. 2005. Interlaboratory comparison of ultrasonic backscatter coefficient measurements from 2 to 9 MHz. *J. Ultrasound Med.* 24:1235–1250.
15. Han, A., R. Abuhabsah, …, W. D. O'Brien, Jr. 2013. The measurement of ultrasound backscattering from cell pellet biophantoms and tumors ex vivo. *J. Acoust. Soc. Am.* 134:686–693.
16. Baddour, R. E., M. D. Sherar, …, M. C. Kolios. 2002. High frequency ultrasound imaging of changes in cell structure including apoptosis. Proceedings of the 2002 IEEE International Ultrasonics Symposium, Munich, Germany, October 8–11.
17. Saha, R. K., and M. C. Kolios. 2011. Effects of cell spatial organization and size distribution on ultrasound backscattering. *IEEE Trans. Ultrason. Ferroelectr. Freq. Control.* 58:2118–2131.